

Electrochemical corrosion behaviour of Sn-Zn-xBi lead-free solder alloys in 0.5 M NaCl solution

Guangyu Liu, Shohreh Khorsand, Shouxun Ji*

Brunel Centre for Advanced Solidification Technology (BCAST), Institute of Materials and Manufacturing, Brunel University London, Uxbridge, Middlesex UB8 3PH, United Kingdom

*Corresponding author. Tel.: +44-1895-266663; Fax: +44-1895-269758; E-mail address: shouxun.ji@brunel.ac.uk.

Abstract:

Electrochemical corrosion behaviour of Sn-3Zn-xBi ($x=0, 1, 3, 5, 7$ wt.%) solder alloys were investigated using potentiodynamic polarization and electrochemical impedance spectroscopy (EIS) techniques, to explore the effect of Bi on corrosion performance of the Sn-Zn alloy. Results indicated that minor (1 wt.%) Bi addition increased the corrosion susceptibility, mainly attributed to the coarsened and more uniformly distributed Zn-rich precipitates, while further increasing Bi decreased the corrosion susceptibility due to the higher fraction of nobler Bi particles serving as anodic barriers. The Sn-3Zn-7Bi possessed the best corrosion resistance among all alloys. The role of Bi on corrosion was considerably discussed.

Keywords:

Sn-Zn-Bi alloy; Corrosion; Polarization; EIS; Zn-rich precipitate; Bismuth

1. Introduction

The lead (Pb)-containing tin (Sn)-based soldering alloys have been extensively used as interconnection and/or packaging components in electronic industries for decades owing to their good solderability, mechanical properties, and low cost [1]. However, with the increasingly concerned problems in environments and health caused by Pb, various alternatives, in particular lead-free Sn-based solders have been developed in recent years. Among them, the eutectic/near-eutectic Sn-Zn alloys have been recognised as appropriate substitutes for Sn-Pb soldering alloys because of the considerable advantages including low melting temperature (198 °C), superior mechanical properties, and low cost [2,3]. Unfortunately, despite the fascinating aspects, the poor corrosion resistance of Sn-Zn alloys has become the major obstacle to achieve further widespread use in electronic assemblies. In reality, solders used in electronic assembly components are directly exposed to air moisture or aggressive medium (e.g. Cl⁻) in industrial environments. This certainly increases the corrosion susceptibility of solder materials and degrade their long-term reliability [4,5]. Especially, the chemical and metallurgical processing can significantly alter the corrosive susceptibility of Sn-Zn alloys [3].

The corrosion behaviour of Sn-Zn alloys in aqueous solution has been the topics of previous investigations. Mendez *et al.* [6] worked on the hypoeutectic Sn-Zn alloys (Zn: <9.0wt.%) with two different types of grain structures: columnar and equiaxed zone, suggesting that the corrosion resistance decreases with increasing the Zn contents. Liu *et al.* [7] investigated the pitting phenomenon of Sn-xZn ($x=6.5, 9.0, 12.0$ wt.%) binary alloys in aerated and quiescent 0.5 M NaCl solution, demonstrating that the pitting susceptibility increases with increasing the Zn contents, which is ascribed to the defects along the intergranular boundaries between Zn-rich phase and Sn matrix. It has been pointed out that the poor corrosion resistance of Sn-Zn alloys is due to the preferential dissolution of Zn-rich phase, which exist in both primary and eutectic phase [8].

Adding alloying elements is deemed an effective way to modify the microstructure, and accordingly, the corrosion resistance of Sn-Zn alloys. Mohanty and Lin [9,10,11,12] reported a series of studies on the electrochemical behaviour of quinary Sn-8.5Zn-Ag-Al-Ga alloys in 3.5 wt.% NaCl solution and found that the alloy exhibits better corrosion resistance than that of binary Sn-8.5Zn alloy. Minor (0.05 wt.%) Ti addition to the Sn-9Zn alloy was reported to enhance the corrosion resistance resulting from the refinement of the Zn-rich precipitates [13]. Also, the addition of intermetallic-forming

elements including Ni, Cr, Cu, and Ag can improve the corrosion resistance of the Sn-9Zn solder alloy [14,15], which was attributed to the decreased volume fraction of coarse Zn-rich precipitates by forming Zn-containing intermetallic phase.

Several alloying elements (e.g. Ni, Al, Ag, Cu, Cr, and Ti) have been considered as additives into Sn-Zn alloys for the purposes of improving the corrosion resistance. However, to the best of our knowledge, limited study has been given to the low-melting point elements such as In and Bi; despite that Ahmido *et al.* [16,17] reported Bi addition could improve the corrosion resistance of Sn-9Zn, but limited explanation for the mechanism. In the present work, Sn-3Zn-*x*Bi (*x*=0, 1, 3, 5, 7 wt.%) solder alloys were prepared, and the electrochemical behaviour was investigated using potentiodynamic polarization and electrochemical impedance spectroscopy (EIS) techniques, aiming to assess the effect of Bi on the corrosion properties of the Sn-Zn alloy. The corrosion mechanism of the Sn-Zn-Bi alloys was studied through microstructure examination on the surface and cross section of the alloys after corrosion measurements, using X-ray diffraction and scanning electron microscopy (SEM) equipped with Energy Dispersive X-ray Analyser (EDS). The discussion is focused on the role of Bi on the corrosion performance.

2. Experimental

2.1 Materials preparation

Sn-3Zn and Sn-3Zn-*x*Bi (*x*=1, 3, 5, and 7 wt.%) alloys were prepared in the present study. Hereafter, the symbol of composition unit wt.% is omitted. The pure Sn, Zn, and Bi ingots with commercial purity (99.9%) were used as the raw materials. Prior to melting, each element was weighed to a specified ratio with specified burning loss compensation. The melt was prepared in a stainless-steel crucible coated with Al₂O₃ coatings and the melting was conducted in an electric resistance furnace. After melting, the melt with temperature around 360 °C was manually poured into a steel mould (preheated at 200 °C) to form casting bars. All the casting bars were 300 mm long and had a trapezoid-shaped cross section of 20×16×16 mm. The chemical compositions of the Sn-Zn-Bi alloys were investigated using inductively coupled plasma atomic emission spectrometry (ICP-AES, ARCOS, Simultaneous ICP Spectrometer, SPECTRO Analytical Instruments GmbH, Germany) and the actual compositions are shown in Table 1.

The specimens for electrochemical measurements were cut along the transverse cross section of casting bars, with a thickness of 8 mm. The working surface was mechanically ground with successive SiC paper from 400 to 4000 grits. The ground surface was then ultrasonically cleaned with distilled water and dried with high pressure air for corrosion tests.

2.2 Electrochemical measurements

Electrochemical measurements were performed using EZstat NuVant Systems Inc. in 0.5 M NaCl solution at room temperature (20 ± 2 °C). The NaCl solution was prepared using analytical grade chemicals and distilled water, and was aerated by direct contact with the laboratory atmosphere. A conventional three-electrode cell configuration was employed to conduct the electrochemical measurements with the Sn-Zn-Bi alloy as working electrode. A Pt spiral wire was used as the counter electrode, and the reference electrode used in this study was saturated calomel electrode (SCE, saturated KCl). Working surface of the electrode exposed to the solution was approximately 1.0 cm². Potentiodynamic polarization curves were acquired by stepping the potential at a scan rate of 0.166 mV/s, from -250 mV to +1000 mV with respect to the OCP. Electrochemical impedance spectroscopy (EIS) curves were obtained at the open circuit potential over a frequency range from 100 mHz -100 kHz with an applied sinusoidal perturbation of 10 mV RMS (root-mean-square) potential. Prior to potentiodynamic polarization and the EIS tests, a 60-min OCP test was conducted to ensure that the working surface has reached a relatively stable state. The experimental EIS spectra were interpreted based on equivalent electrical circuit using the program Zview to obtain the fitting parameters.

2.3 Microstructure characterisation

The chemical compositions of the alloys were analysed using the inductively coupled plasma atomic emission spectroscopy (ICP-AES, ARCOS, Simultaneous ICP Spectrometer, SPECTRO Analytical Instruments GmbH, Germany). Microstructure of as-prepared alloys and corrosion products after polarization measurements were examined using a Zeiss Supra 35VP scanning electron microscopy (SEM) equipped with Energy Dispersive X-ray Analyser (EDS). Moreover, X-ray diffraction (XRD) for phase identification of the corrosion products was carried out using Rigaku D/max 2550 diffractometer with $\text{CuK}\alpha$ radiation.

3. Results

3.1 Microstructure of Sn-3Zn-xBi alloys

Figure 1 shows the typical microstructure of as-prepared Sn-3Zn-xBi alloys prior to electrochemical measurements. The microstructure of the hypoeutectic Sn-3Zn (Figure 1a) mainly consisted of light grey β -Sn phase exhibiting dendrites morphology and Sn-Zn eutectic in the form of alternate distribution of Sn phase and dark Zn-rich needles with very small spacing (inset). Similar microstructure was reported in hypoeutectic Sn-6.5Zn alloy [18]. By adding 1-7 wt.% of Bi, the microstructure was largely changed in terms of the morphology, size, and distribution of both primary β -Sn phase and eutectics, comprising β -Sn phase, Zn-rich phase and white Bi particles [19]. Notably, misaligned Zn-rich phase in the form of relatively coarse flakes instead of well-aligned small Zn-rich needles was largely observed in Bi-containing Sn-3Zn-xBi alloys. More Bi addition lead to more Bi aggregates and those were located close to Zn-rich precipitates, with individual particle size being approximately $1\mu\text{m}$ (Figure 1f).

3.2 Potentiodynamic polarization curves

Figure 2 shows the potentiodynamic polarization curves of Sn-3Zn and Sn-3Zn-xBi ($x=1, 3, 5,$ and 7 wt.%) alloys in 0.5 M NaCl solution. It was seen that all the Sn-3Zn-xBi alloys exhibited similar corrosion behaviour, evidenced by similar polarization curves. Since polarization measurements were conducted in a stagnant and naturally aerated NaCl solution at room temperature, the cathodic branch (AB) of polarization could be ascribed to the reaction with the dissolved oxygen [20]: $\text{O}_2 + 2\text{H}_2\text{O} + 4\text{e}^- \rightarrow 4\text{OH}^-$. On scanning in the anodic direction to BC stage, all the alloys exhibited sharp increases in anodic current density attributable mainly to the active dissolution of Zn phase [12]. Afterwards, in the range of CD, the alloys showed typical passivation behaviour in which the current density decreased gradually as the working electrode was anodically polarized toward a more positive potential. This could be attributed to the formation of Zn and/or Sn oxide or hydroxides [21,22]. These oxides act as barrier layers to inhibit further dissolution of the alloys. It should be noted that the film formed in the CD region is not a protective film. After point D, the current density increased again, corresponding to the breakdown of the passive layers.

The detailed electrochemical parameters are summarised in Table 2. The corrosion current density (i_{corr}) was obtained by extrapolating the cathodic Tafel region back to the corrosion potential (E_{corr}) [23]. It was obvious that the Sn-3Zn-1Bi alloy possessed higher values of i_{corr} compared with that of the Sn-3Zn alloy, suggesting a lower corrosion resistance after a small amount (1 wt.%) of Bi addition. However, in the Bi-containing Sn-3Zn-xBi alloys, the corrosion resistance increased continuously with increasing the Bi contents, which was evidenced by the fact that the value of i_{corr} decreased constantly from 17.4 uA.cm^{-2} to 8.7 uA.cm^{-2} as Bi contents was increased from 1 wt.% to 7 wt.%. Interestingly, when Bi was increased to 5 wt.% the Sn-3Zn-5Bi exhibited same level of value (13.4 uA.cm^{-2}) of i_{corr} with that of Sn-3Zn alloy (13.5 uA.cm^{-2}), indicating the similar capability of corrosion resistance. The Sn-3Zn-7Bi alloy showed the lowest i_{corr} which indicates the highest corrosion resistivity among these alloys. Additionally, the critical current density (i_{cc}) and passivation current density (i_{pass}) exhibited a similar variation trend with that of i_{corr} , further confirming the consistency of measurement. Hence, according to the potentiodynamic polarization results, it could be

concluded that the corrosion resistance decreased in the order of Sn-3Zn-7Bi > Sn-3Zn-5Bi ≥ Sn-3Zn > Sn-3Zn-3Bi > Sn-3Zn-1Bi.

3.3 Electrochemical impedance spectroscopy

Figure 3 shows the Nyquist and Bode plots of Sn-3Zn-*x*Bi (*x*=0, 1, 3, 5 and 7 wt.%) alloys in 0.5 M NaCl solution at their open circuit potential. It was observed that each Nyquist plot was composed of two depressed capacitive semi-arcs (Figure 3a). The Sn-3Zn-1Bi alloy displayed a smallest arc radius, indicating the lowest corrosion resistance among these alloys. Also, larger capacitive arc radius appeared in the Bi-containing Sn-3Zn-*x*Bi alloy with higher Bi contents. Plus, the Bode plots of $|Z|$ vs. frequency (Figure 3c) revealed that more Bi contents resulted in the higher value of impedance, suggesting that Bi addition could increase the corrosion resistance of Sn-3Zn-*x*Bi alloys (*x*=1, 3, 5, and 7 wt.%). It is noted that these phenomena were in line with the results shown by polarization measurements. The Bode phase plot (Figure 3d) indicated two time constant in the impedance spectra, corresponding to two capacitive loops in Figure 3a. The first time constant at medium-high frequencies (80-400 Hz) could be correlated with the dielectric behaviour of the porous layer with respect to the solution/porous film interface reactions, and the second one at low frequencies (0.1-0.3 Hz) corresponded to the passive layer related to charge transfer resistance at the passive film/alloy interface [24].

Figure 4 shows two different equivalent circuits (ECs) which were used in this study to fit the experimental points. The fitted EIS results are summarised in Table 3. The goodness of fit was evaluated with the chi-squared (χ^2) values, which in all cases was in the order of 10^{-4} - 10^{-3} . Also, a good agreement was observed between the experimental points and the fitting curves, denoted as scattered symbols and solid lines, respectively (Figure 3). In the ECs, R_s represents the uncompensated electrolyte resistance. As can be seen in Figure 3, real systems do not behave as an ideal capacitor, therefore, a constant phase element (CPE) instead of a pure capacitor in the equivalent circuit was used to fit the impedance behaviour more accurately. In general, the constant phase element (CPE) is associated with the distributed surface reactivity, inhomogeneity, roughness, adsorption of species and electrode porosity [25]. R_1 and CPE_1 represent the resistance and capacitance of the corrosion product layer. R_{ct} represents the charge transfer resistance with respect to the passive layer/alloy interface and CPE_{dl} is the double layer capacitance; W represents the Warburg impedance describing the interface diffusion of charge species.

It was evidenced from Table 3 that the charge transfer impedance (R_{ct}) of Sn-3Zn-1Bi was much lower than that of Sn-3Zn. However, pronounced increases of R_{ct} was observed in Bi-containing alloys with increasing the Bi contents from 1 wt.% to 7 wt.%, indicating that the charge transfer process occurred in higher difficulty by adding more Bi. Interestingly, adding 7 wt.% Bi resulted in the presence of diffusion-controlled impedance, which might indicate that the corrosion mechanism of the modified alloy was controlled by both charge transfer and diffusion process. Note that, the existence of transport resistance (R_w) showed that the transport process of charge species occurred much more difficult in the Sn-3Zn-7Bi alloy. According to the ECs (neglect the solution resistance), total impedance (R_t) can be extracted from R_1 , R_{ct} and R_w (diffusion resistance), to evaluate the overall corrosion resistance. The Sn-3Zn exhibited a large value of R_t , 969.5 Ω cm². When small amount of Bi was added, the total impedance of Sn-3Zn-1Bi and Sn-3Zn-3Bi alloys showed lower values of R_t , indicating a worse corrosion resistance. However, the R_t value for Sn-3Zn-5Bi and Sn-3Zn-7Bi was relatively large, approximately 1178.5 and 2265 Ω cm², respectively, suggesting an enhanced corrosion resistance with a higher amount of Bi addition. It was clear that the Sn-3Zn-7Bi exhibited the highest corrosion resistance among these alloys. Thus, based on the EIS results, it is further confirmed that the corrosion resistance increased in the sequence of Sn-3Zn-1Bi, Sn-3Zn-3Bi, Sn-3Zn, Sn-3Zn-5Bi, and Sn-3Zn-7Bi. This is in agreements to the results proved by polarization measurements.

3.4 Corrosion products characterization

3.4.1 Surface characterization

Figure 5 shows the typical SEM micrograph and element mapping of the surface of Sn-3Zn after polarization measurement. The severely corroded area denoted by the dark contrast (Figure 5a) was mainly composed of Cl, O, and Zn elements, indicating that corrosion products were predominantly made of Cl, O, and Zn. The slightly-/non- corroded area represented by the light contrast in Figure 5a was covered with numerous Sn and a small amount of O. It was thus deduced that Zn phase instead of Sn was selectively and preferentially corroded under the engagement of Cl⁻ and OH⁻ anions.

Figure 6 presents the XRD patterns of the surface of Sn-3Zn-*x*Bi (*x*=0, 1, 3, 5, and 7 wt.%) alloys after polarization measurements, for the purposes of confirming the phase composition of corrosion products. It was seen that there was still β-Sn phase remained after polarization measurements in all cases, while Zn phase was scarcely detected, further revealing that Zn-rich phase was heavily consumed. Bi phase was extensively detected in the Bi-containing alloys with Bi contents being more than 1wt.%, confirming the difficulty of Bi in being corroded in 0.5 M NaCl solution due to its relatively higher corrosion potential compared with Sn and Zn [26]. The main corrosion product for all Sn-3Zn-*x*Bi alloys was identified as a complexed Zn hydroxyl chloride hydrates, namely simonkolleite Zn₅(OH)₈Cl₂·H₂O. Plus, a trace amount of ZnO was discovered as well.

Figure 7 presents the typical SEM micrograph and EDS analysis illustrating the surface morphology and corresponding chemical composition of corrosion products of Sn-3Zn after polarization measurement. From Figure 7a and b, the corroded region was covered with sparsely aggregated plate-like structures, which were confirmed simonkolleite Zn₅(OH)₈Cl₂·H₂O by EDS analysis on spectrum S1. This was in agreements with the XRD Results. Zooming in the initial eutectic region (Figure 7c), it was seen that the initial Zn-rich needles were dissolved and depleted, leaving narrow channels on the surface, whereas the initial β-Sn phase in the eutectic region remained, as demonstrated by EDS analysis on spectrum S2, further indicating the easier destruction of Zn-rich phase compared to β-Sn phase. Furthermore, the corrosion product exhibiting a ball-shaped morphology was observed, which was found the aggregate of the ZnO plates (EDS analysis on S3). These ball-like ZnO products have been previously reported by other researchers on the study of Sn-Zn alloys after immersion corrosion [8].

Figure 8a and 8b presents the SEM micrograph of the surface of the Bi-containing Sn-3Zn-1Bi and Sn-3Zn-5Bi alloys after polarization measurements in 0.5 M NaCl solution, respectively. From Figure 8a, many Bi particles were seen to remain on the surface, as shown by arrows. These particles were confirmed Bi particles by EDS analysis (not present here). Surrounding the Bi particle, Sn phase was selectively corroded, suggesting appearance of micro-galvanic couples between the β-Sn phase and the Bi phase. For certain sites (dashed circle), Bi particles were depleted because the neighbouring β-Sn matrix was severely consumed and thus the interface bonding was consequently damaged. Also, pits and micro-cracks were observed in the corroded surface of Sn-3Zn-5Bi alloy, which might indicate weak protection of the corrosion product layers (Figure 8b). Note that, pits and micro-cracks were observed not only in the case of Sn-3Zn-5Bi but in all Sn-3Zn-*x*Bi (*x*=0, 1, 3, 5, and 7 wt.%) alloys

3.4.2 Cross section characterization

For a better understanding of pitting corrosion process, cross section characterization was further carried out after corrosion measurement. Figure 9 shows the cross-section SEM micrograph and the element mapping of a typical pit of the Sn-3Zn-5Bi alloy after polarization measurement. The result of element mapping confirmed the strong presence of Cl, O, and Zn in the pit, suggesting that anions including Cl⁻ and OH⁻ had migrated inwards the alloy along the initial Zn-rich precipitates. It was thus concluded that Zn-rich precipitates could provide preferential transport paths for Cl⁻ and OH⁻ penetration. Notably, Bi phase was scarcely identified by the element mapping (Figure 9f), indicating that this individual pit initiated and propagated without participant Bi phase.

Closer inspection of the pit (Figure 9a1), the major pitting product was found Zn₅(OH)₈Cl₂·H₂O, which was confirmed by the EDS results. Interestingly, the pitting product, Zn₅(OH)₈Cl₂·H₂O, exhibited a porous interlinked network structure. A similar porous network-structured corrosion

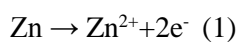
product was also reported on the study of Sn-Zn [8]. The pores could provide ease of transport of Cl^- and OH^- from solution inwards the interior of the alloys. In this way, a continuous complement of poisonous anions (e.g. Cl^-) was delivered, thus, promoting the pitting propagation. In the meantime, localized cracks/breakdown appeared as well. The crack on one hand provided the channel for the penetration of corrosive medium (Cl^- and OH^-); on the other hand, the crack could increase the chances of removal of pitting products away from the surface, increasing the possibility of anions in the solution diffusing towards the alloys, which promoted the pitting rate kinetically.

Figure 10 shows the cross-section SEM micrograph and the element mapping of another typical type of pits in Sn-3Zn-5Bi after polarization measurement. It was observed that the pit was covered with Cl, O, Sn, and Bi elements. A similar conclusion could be drawn that the pitting initiation and subsequent propagation were resulted from migration of attacking Cl^- and OH^- anions inwards the alloy. EDS results (Figure 10b and c) confirmed that pitting products contained SnO and the Sn hydroxyl chloride hydrate compounds, $\text{Sn}_3\text{O}(\text{OH})_2\text{Cl}_2$. Different from the previously mentioned pit, the Zn-rich precipitate was barely identified here, while numerous Bi particles were largely detected in this pit (Figure 10d). Thus, the pitting susceptibility could be enhanced in the sites where large amounts of Bi particles assembled. This could be related to the formation of the Bi/Sn galvanic couples which will be discussed next.

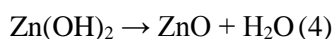
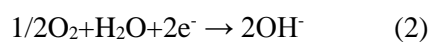
4. Discussion

Based on the polarization and EIS results, it has been confirmed that a small amount (1 and 3 wt.%) of Bi addition to the Sn-3Zn alloys could cause decreased corrosion resistance. However, when Bi contents was further increased to 5 and 7 wt.%, the Sn-3Zn-xBi ($x=5$, and 7 wt.%) alloys exhibited higher corrosion resistance than that of Sn-3Zn. Furthermore, for Bi-containing Sn-3Zn-xBi alloys the corrosion resistance increased with increasing Bi contents from 1 wt.% to 7 wt.% and the Sn-3Zn-7Bi alloy showed the best corrosion resistance among them. This could be associated with: (1) the microstructure modification through addition of Bi with respect to the morphology, size, and distribution of the Zn-rich precipitates; (2) the additional micro-galvanic effect caused by Bi particles; and (3) the barrier effect of Bi phase.

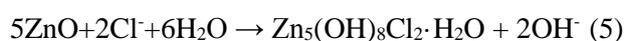
In the Sn-Zn system since Zn exhibits more negative electrode potential (-0.763 V vs. SHE) than Sn (-0.136 V vs. SHE) the Zn-rich precipitates act as active anodes and can be preferentially corroded under corrosive circumstances [27]. The corrosion process begins with the dissolution of Zn at anodic sites:



In this way, the initial Zn-rich precipitates could be selectively consumed, leaving the β -Sn phase (cathode) remained (Figure 7c). With participation of the water and oxygen further electrochemical reactions take place, forming zinc hydroxide and/or zinc oxide:



In the presence of Cl^- , especially when the chloride concentration is higher than 0.1 M, Cl^- will move towards Zn dissolution sites, causing gradual formation of insoluble zinc hydroxychloride, $\text{Zn}_5(\text{OH})_8\text{Cl}_2 \cdot \text{H}_2\text{O}$ [28]:



These corrosion products, ZnO and $\text{Zn}_5(\text{OH})_8\text{Cl}_2 \cdot \text{H}_2\text{O}$ were readily recognised by the XRD results (Figure 6) and EDS composition analysis (Figure 7b). In this sense, $\text{Zn}_5(\text{OH})_8\text{Cl}_2 \cdot \text{H}_2\text{O}$ is thus

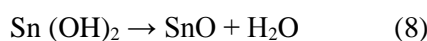
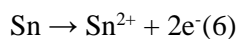
expected to precipitate close to the anodic sites, i.e., Zn-rich precipitates, which was in deed the case denoted by the pit shown in Figure 9.

In the case of Sn-3Zn, the Zn-rich precipitates displayed as small-sized needle-shaped morphologies and these Zn-rich needles were located at the Sn-Zn eutectic cells/regions. Accordingly, the eutectic regions could be reasonably regarded as the corrosion-vulnerable sites at which anodic Zn-rich phase was dissolved and depleted, while the primary β -Sn cells could be considered as the cathodic noble locations where corrosion could rarely occur. This was supported by the surface examination and composition analysis of Sn-3Zn after polarization measurements (Figure 7c).

When Bi was added, i.e., in the case of Sn-3Zn- x Bi ($x=1, 3, 5,$ and 7 wt.%) alloys, Zn-rich precipitates were dramatically increased in dimensions, and its distribution became more uniform. Those in larger size could lead to degradation of corrosion performance due to the weak bond between the coarse Zn-rich precipitates and β -Sn matrix. This was based on the idea that defects (e.g. dislocations or voids) could be easily accumulated near the interface between the coarse Zn-rich precipitate and the Sn phase [29,30]. The defects-accumulated sites could thus benefit transport of Cl^- or OH^- inwards and promote chemical reaction between anions and the Zn-rich phase, accelerating the corrosion rates. Meanwhile, the pitting can be highly prone to initiate and propagate along the vulnerable Zn/Sn interface, which was reflected from the pit microstructure shown in Figure 9. Similar phenomenon was reported by Liu *et al.* [13] who has demonstrated that the corrosion resistance is enhanced after addition of trace amount of Ti to the Sn-9Zn alloy attributed to elimination of large Zn-rich precipitates.

Also, in the Sn-3Zn alloy the corrosion-vulnerable sites, i.e., Sn-Zn eutectic “islands”, were geographically and largely isolated by a large proportion of primary β -Sn dendrites serving as noble cathodes (Figure 1a). This means that noble β -Sn phase can act as the barrier, causing obstruction of corrosion [31]. On the contrary, in the Bi-containing Sn-3Zn- x Bi alloys, a much more uniform distribution of the Zn-rich precipitates appeared, which means that more proportion of corrosion-vulnerable sites presented and fewer fractions of effective anodic barriers exhibited. Consequently, the Sn-3Zn- x Bi ($x=1,$ and 3 wt.%) alloys presented higher corrosion susceptibility in comparison with the Sn-3Zn alloy.

It is worthy of note that in addition to the effect attributable to the change of the Zn-rich precipitate with respect to its size and distribution, the Bi particle itself played a crucial role in affecting the corrosion resistance of the alloys. The effect caused by Bi particles may involve two aspects: galvanic effect and anodic barrier. When a small amount of Bi (1 wt.%) was added to Sn-3Zn, Bi particles were randomly aggregated and discretely dispersed in the Sn matrix and majority of those were located near Zn-rich precipitates, as shown in Figure 1b and c. Extra micro-galvanic couples, i.e., β -Sn phase/Bi phase and Zn-rich phase/Bi phase, may form, due to Bi phase possessing the highest electrode potential (0.293 V *vs.* SHE) compared with Sn (-0.136 V *vs.* SHE) and Zn (-0.763 V *vs.* SHE). Therefore, in the β -Sn/Bi micro-galvanic couples the β -Sn could be selectively resolved as the anodes, leaving Bi remained (Figure 8a), causing formation of corrosion products, SnO and $\text{Sn}_3\text{O}(\text{OH})_2\text{Cl}_2$ (Figure 10). Possible chemical reactions involve [5,32]:



In this way, the additional galvanic effect could have a negative effect on the corrosion resistance of Sn-Zn alloys. However, it worthy noted that the detrimental galvanic effect caused by β -Sn/Bi micro-galvanic couple was believed to be minimal because the corrosion potential difference between Bi and Sn is small [26]. This was also reflected by the fact that no clear peaks corresponding to the corrosion products, SnO and/or $\text{Sn}_3\text{O}(\text{OH})_2\text{Cl}_2$, were identified in the XRD results of the corroded surface of the

Bi-containing Sn-3Zn-xBi alloys. Therefore, the galvanic corrosion theory which gives the idea that larger ratio of cathodic to anodic would lead to a severer corrosion of the anode alloy, resulting more damage during electrochemical measurement, might be not applicable in the case of Bi-containing Sn-3Zn-xBi alloys.

On the contrary, the noble barrier effect of cathodic Bi phase operates more significantly than the galvanic cathode, leading to the increased corrosion resistance with more Bi particles. Similar phenomenon was reported in Mg alloys where the $Mg_{17}Al_{12}$ (β phase) has two influences on corrosion, as a galvanic cathode and as a barrier, depending on the volume fraction of $Mg_{17}Al_{12}$ in the Mg matrix [33,34]. The $Mg_{17}Al_{12}$ phase mainly serves as a galvanic cathode and accelerates the corrosion process of matrix if the volume fraction of $Mg_{17}Al_{12}$ phase was small. However, for a higher volume fraction, the $Mg_{17}Al_{12}$ phase may act as an anodic barrier to inhibit the overall corrosion of the alloy. Also, Osorio *et al.* [35] reported that in the Al-1.5 wt.% Fe alloy more extensive distribution of Al_6Fe particles provides a better protective effect with the nobler intermetallic Al_6Fe particles “enveloping” the anodic Al-rich phase, resulting in better corrosion resistance. Notably, with increasing the Bi contents from 1 wt.% to 7 wt.%, the volume fraction of Bi particles was observed to be largely increased and those became better connected from each other, forming the noble barriers or “enveloping” against corrosion. Based on this, it was deduced that a larger proportion of Bi networks acting as anodic barriers in Sn-3Zn-xBi alloys with higher Bi contents was the reason for the correspondingly increased corrosion resistance.

5. Conclusions

In the present study, the effect of Bi on the corrosion performance of the Sn-Zn alloy was investigated using potentiodynamic polarization and electrochemical impedance spectra (EIS) techniques. Based on the results of electrochemical measurements and microstructure examination, main conclusions could be drawn as follows:

- (1) In the Sn-3Zn-xBi system, the Zn-rich phase possessing the lowest corrosion potential among all phases serves as the anodic and thus is selectively and preferentially corroded. The corrosion products are plate-like $Zn_5(OH)_8Cl_2 \cdot H_2O$.
- (2) A small amount (1 wt.%) of Bi addition to the Sn-3Zn alloy can increase the corrosion susceptibility, which has been ascribed to the microstructure modification with respect to the coarsen and more uniformly distributed Zn-rich phase.
- (3) The β -Sn/Bi micro-galvanic effect is deemed minor due to the small potential difference between Bi phase and Sn phase. Thus, the galvanic effect caused by Bi particle has little effect on the corrosion resistance.
- (4) In Bi-containing Sn-3Zn-xBi alloys, with increasing the Bi contents from 1 wt.% to 7 wt.%, the corrosion resistance is constantly increased due to the increase of barrier effect of Bi phase to counteract the detrimental effect resulted from the coarsen Zn-rich precipitates.

Acknowledgment

Financial support from the National Aerospace Technology Exploitation Programme (NATEP) and Chemring Energetics UK [grant number WEA058] is gratefully acknowledged.

Table 1. Chemical composition of the experimental Sn-Zn-Bi alloys analysed by inductively coupled plasma atomic emission spectroscopy (ICP-AES), wt.%.

Alloys	Zn	Bi	Ni	Cu	Fe	Sb	As	Cd	Sn
Sn-3Zn	3.11	0.03	0.01	0.015	0.01	0.02	0.014	0.006	Rem.
Sn-3Zn-1Bi	2.89	0.98	0.01	0.012	0.01	0.02	0.008	0.006	Rem.
Sn-3Zn-3Bi	3.01	3.15	0.01	0.011	0.01	0.02	0.009	0.005	Rem.
Sn-3Zn-5Bi	3.09	5.21	0.01	0.016	0.01	0.03	0.012	0.007	Rem.
Sn-3Zn-7Bi	2.95	6.93	0.01	0.013	0.01	0.02	0.009	0.005	Rem.

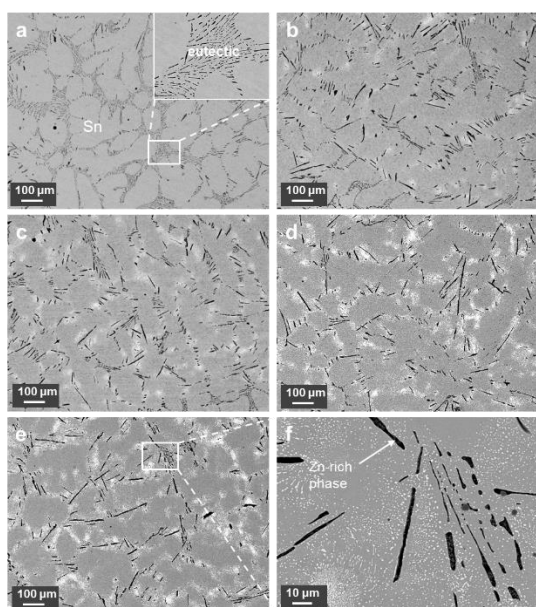


Figure 1 Backscattered SEM micrographs showing the microstructure of Sn-Zn-Bi alloys prior to electrochemical measurements: (a)Sn-3Zn, (b)Sn-3Zn-1Bi, (c) Sn-3Zn-3Bi, (d)Sn-3Zn-5Bi, and (e, f) Sn-3Zn-7Bi

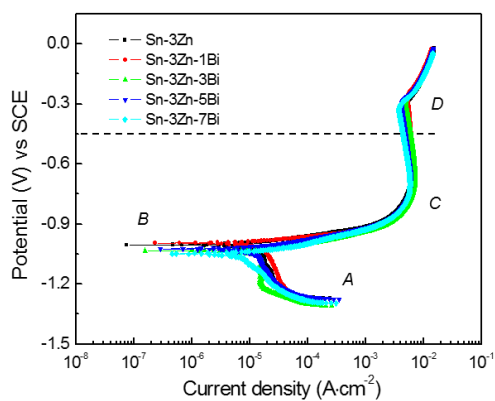


Figure 2. Potentiodynamic polarization curves of Sn-3Zn-xBi (x=0, 1, 3, 5, and 7wt.%) alloys after 60-min immersion in 0.5M NaCl solution.

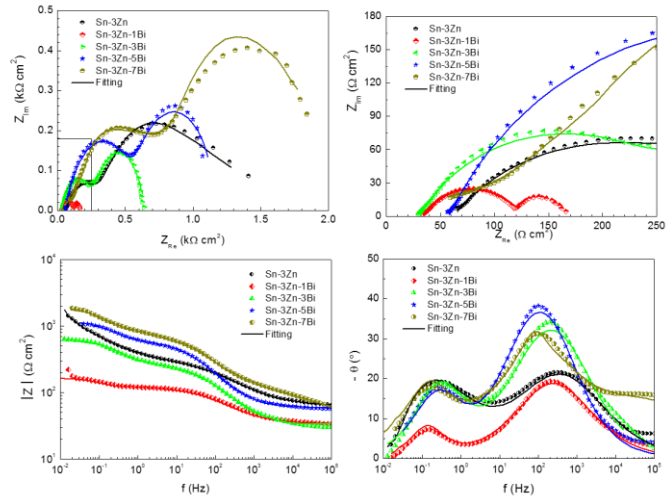


Figure 3 Electrochemical impedance spectra of Sn-3Zn-xBi ($x=0, 1, 3, 5,$ and 7 wt.%) alloys under the open circuit potential after 30 min immersion in 0.5 M NaCl solution: (a) Nyquist plots; (b) high frequency part of the Nyquist plots; (c) Bode Z plots (modulus vs f); (d) Bode phase plots (phase angle vs f).

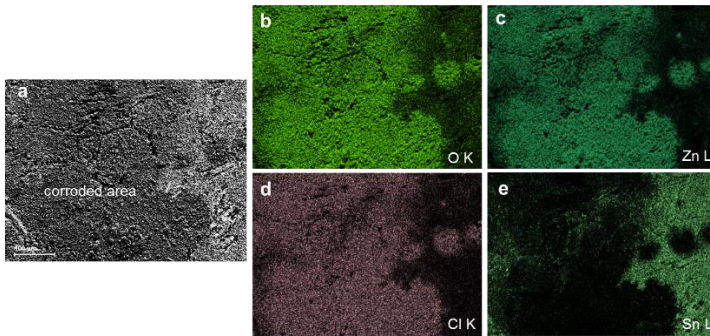


Figure 5 SEM-BSE micrograph of the surface and element mapping for the Sn-3Zn alloy after polarization measurements in 0.5 M NaCl solution.

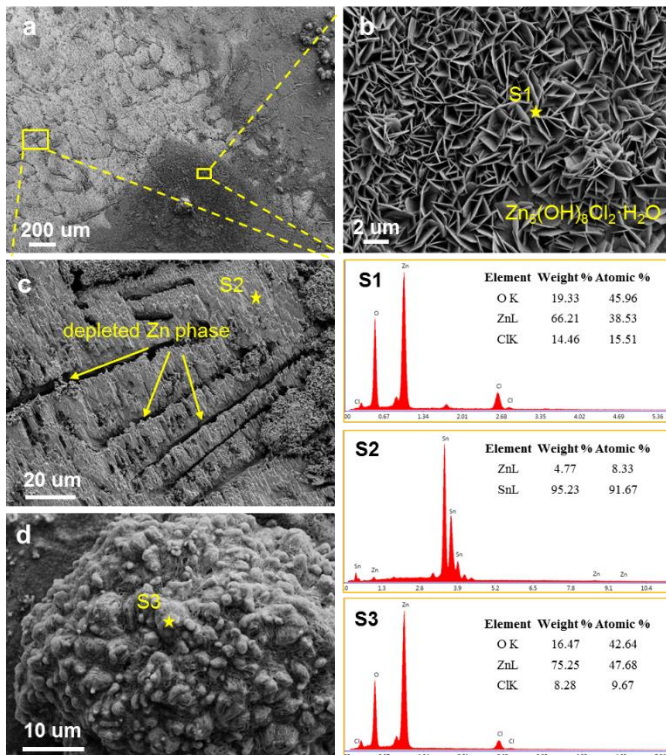


Figure 7 SEM micrographs with different magnification of Sn-3Zn alloy after polarization measurements in 0.5 M NaCl solution. The EDS result is corresponding to the spectrums in b, c, and d (S1, S2, and S3).

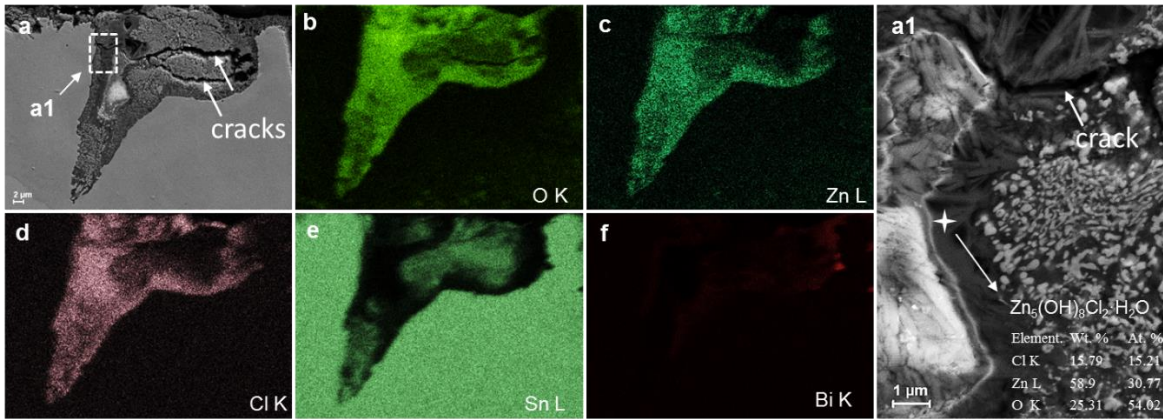


Figure 9 SEM-BSE micrograph of the cross section and element mapping for Sn-3Zn-5Bi alloy after polarization measurements in 0.5 M NaCl solution.

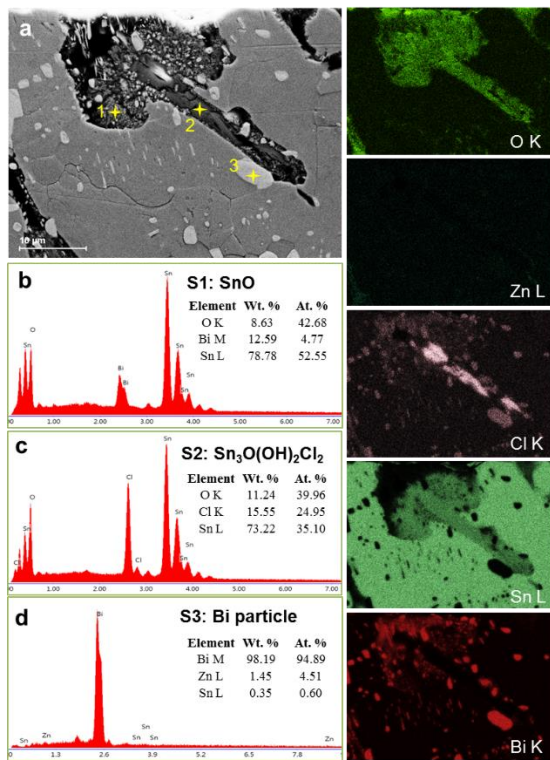


Figure 10. SEM-BSE micrograph of the cross section and element mapping for Sn-3Zn-5Bi alloy after polarization measurements in 0.5 M NaCl solution.

Reference

- [1] R.A. Islam, B.Y. Wu, M.O. Alam, Y.C. Chan, W. Jillek, Investigations on microhardness of Sn-Zn based lead-free solder alloys as replacement of Sn-Pb solder, *J. Alloys Compd.* 392 (2005) 149-158.
- [2] X. Wei, H. Huang, L. Zhou, M. Zhang, X. Liu, On the advantages of using a hypoeutectic Sn-Zn as lead-free solder material, *Mater. Lett.* 61 (2007) 655-658.
- [3] K. Sukanuma, K.S. Kim, Sn-Zn low temperature solder, *J. Mater. Sci.* 18 (2007) 121-127.
- [4] M. Abteu, G. Selvaduray, Lead-free solders in microelectronics, *Mater. Sci. Eng. R. Rep.* 27 (2000) 95-141.
- [5] D. Li, P.P. Conway, C. Liu, Corrosion characterization of tin-lead and lead-free solders in 3.5 wt.% NaCl solution, *Corros. Sci.* 50 (2008) 995-1004.

-
- [6] C.M. Méndez, V.L. Scheiber, R.S. Rozicki, A.I. Kociubczyk, A.E. Ares, Electrochemical behaviour of Sn-Zn alloys with different grain structures in chloride-containing solutions, *Arabian Journal of Chemistry* (2017), In press.
- [7] J.C. Liu, S.W. Park, S. N. M. Nogi, H. Koga, J.S. Ma, G. Zhang, K. Suganuma, The role of Zn precipitates and Cl⁻ anions in pitting corrosion of Sn-Zn solder alloys, *Corros. Sci.* 92 (2015) 263-271.
- [8] J.C. Liu, Z.H. Wang, J.Y. Xie, J.S. Ma, G. Zhang, K. Suganuma, Understanding corrosion mechanism of Sn-Zn alloys in NaCl solution via corrosion products characterization, *Mater. Corros.* 67 (2016) 522-530.
- [9] U.S. Mohanty, K.L. Lin, Electrochemical corrosion behaviour of lead-free Sn-8.5 Zn-XAg-0.1 Al-0.5 Ga solder in 3.5% NaCl solution, *Mater. Sci. Eng. A* 406 (2005) 34-42.
- [10] U.S. Mohanty, K.L. Lin, The polarization characteristics of Pb-free Sn-8.5 Zn-XAg-0.1 Al-0.05 Ga alloy in 3.5% NaCl solution, *Corros. Sci.* 49 (2007) 2815-2831.
- [11] U.S. Mohanty, K.L. Lin, The effect of alloying element gallium on the polarization characteristics of Pb-free Sn-Zn-Ag-Al-XGa solders in NaCl solution, *Corros. Sci.* 48 (2006) 662-678.
- [12] U.S. Mohanty, K.L. Lin, Electrochemical corrosion behaviour of Pb-free Sn-8.5 Zn-0.05 Al-XGa and Sn-3Ag-0.5 Cu alloys in chloride containing aqueous solution, *Corros. Sci.* 50 (2008) 2437-2443.
- [13] J.C. Liu, G. Zhang, J.S. Ma, K. Suganuma, Ti addition to enhance corrosion resistance of Sn-Zn solder alloy by tailoring microstructure, *J. Alloys Compd.* 644 (2015) 113-118.
- [14] T.C. Chang, M.H. Hon, M.C. Wang, D.Y. Lin, Electrochemical behaviours of the Sn-9Zn-xAg lead-free solders in a 3.5 wt% NaCl solution, *J. Electrochem. Soc.* 151 (2004) 484-491.
- [15] J.C. Liu, Z.H. Wang, J.Y. Xie, J.S. Ma, Q.Y. Shi, G. Zhang, K. Suganuma, Effects of intermetallic-forming element additions on microstructure and corrosion behavior of Sn-Zn solder alloys, *Corros. Sci.* 112 (2016) 150-159.
- [16] A. Ahmido, S. El Hajjaji, B. Ouaki, A. Sabbar, S. Sebbahi, Corrosion behavior of Sn-9Zn-xBi lead-free solder alloys in NaCl 3% solution, *Mater.Sci. An Indian Journal* 13 (2015) 69-76.
- [17] A. Ahmido, A. Sabbar, H. Zouihri, K. Dakhsi, F. Guedira, M. Serghini-Idrissi, S. El Hajjaji, Effect of bismuth and silver on the corrosion behaviour of Sn-9Zn alloy in NaCl 3 wt.% solution, *Mater. Sci. Eng. B* 176 (2011) 1032-1036.
- [18] A.A. El-Daly, A.E. Hammad, G.A. Al-Ganainy, A.A. Ibrahim, Enhancing mechanical response of hypoeutectic Sn-6.5 Zn solder alloy using Ni and Sb additions, *Mater. Des.* 52 (2013) 966-973.
- [19] A.A. El-Daly, H.A. Hashem, N. Radwan, F. El-Tantawy, T.R. Dalloul, N.A. Mansour, H.M. Abd-Elmoniem, E.H. Lotfy, Robust effects of Bi doping on microstructure development and mechanical properties of hypoeutectic Sn-6.5Zn solder alloy, *J. Mater. Sci. Mater. in Electron.* 27 (2016) 2950-2962.
- [20] U.S. Mohanty, K.L. Lin, Potentiodynamic polarization measurement of Sn-8.5 Zn-XAl-0.5 Ga alloy in 3.5% NaCl solution, *J. Electrochem. Soc.* 153 (2006) B319-B324.
- [21] S. Chung, J. Cheng, S. Chiou, H. Shih, EIS behaviour of anodized zinc in chloride environments, *Corros. Sci.* 42 (2000) 1249-1268.
- [22] S. Kapusta, N. Hackerman, Anodic passivation of tin in slightly alkaline solutions, *Electrochim. Acta* 25 (1980) 1625-1639.
- [23] E. McCafferty, Validation of corrosion rates measured by the Tafel extrapolation method, *Corros. Sci.* 47 (2005) 3202-3215.
- [24] F. Mansfeld, Electrochemical impedance spectroscopy (EIS) as a new tool for investigating methods of corrosion protection, *Electrochim. Acta* 35 (1990) 1533-1544.
- [25] G.J. Brug, A.L.G. Van Den Eeden, M. Sluyters-Rehbach, J.H. Sluyters, The analysis of electrode impedances complicated by the presence of a constant phase element. *J. Electroanal. Chem. Interfacial Electrochem.* 176 (1984) 275-295.
- [26] M. Mori, K. Miura, T. Sasaki, T. Ohtsuka, Corrosion of tin alloys in sulfuric and nitric acids, *Corros. Sci.* 44 (2002) 887-898.
- [27] Z. Wang, Electrochemical behaviour of Zn-xSn high-temperature solder alloys in 0.5M NaCl solution, *J. Alloys Compd.* 716 (2017) 231-239.
- [28] T. Falk, J.E. Svensson, L.G. Johansson, The influence of CO₂ and NaCl on the atmospheric corrosion of zinc a laboratory study, *J. electrochem. Soc.* 145 (1998) 2993-2999.
- [29] L.R. Garcia, W.R. Osorio, L.C. Peixoto, A. Garcia, Mechanical properties of Sn-Zn lead-free solder alloys based on the microstructure array, *Mater. Charact.* 61 (2010) 212-220.
- [30] K. Prabhu, P. Deshapande, Effect of cooling rate during solidification of Sn-9Zn lead-free solder alloy on its microstructure, tensile strength and ductile-brittle transition temperature, *Mater. Sci. Eng. A* 533 (2012) 64-70.
- [31] G. Song, A. Atrens, Understanding magnesium corrosion-A framework for improved alloy performance, *Adv. Eng. Mater.* 5 (2003) 837-858.
- [32] S.D. Kapusta, N. Hackerman, Anodic passivation of tin in slightly alkaline solutions, *Electrochim. Acta* 25 (1980) 1625-1639.
- [33] G. Song, A. Atrens, X. Wu, B. Zhang, Corrosion behaviour of AZ21, AZ501 and AZ91 in sodium chloride, *Corros. Sci.* 40 (1998) 1769-1791.
- [34] G. Song, A. Atrens, M. Dargusch, Influence of microstructure on the corrosion of diecast AZ91D, *Corros. Sci.* 41 (1999) 249-273.
- [35] W.R. Osório, L.C. Peixoto, P.R. Goulart, A. Garcia, Electrochemical corrosion parameters of as-cast Al-Fe alloys in a NaCl solution, *Corros. Sci.* 52 (2010) 2979-2993.